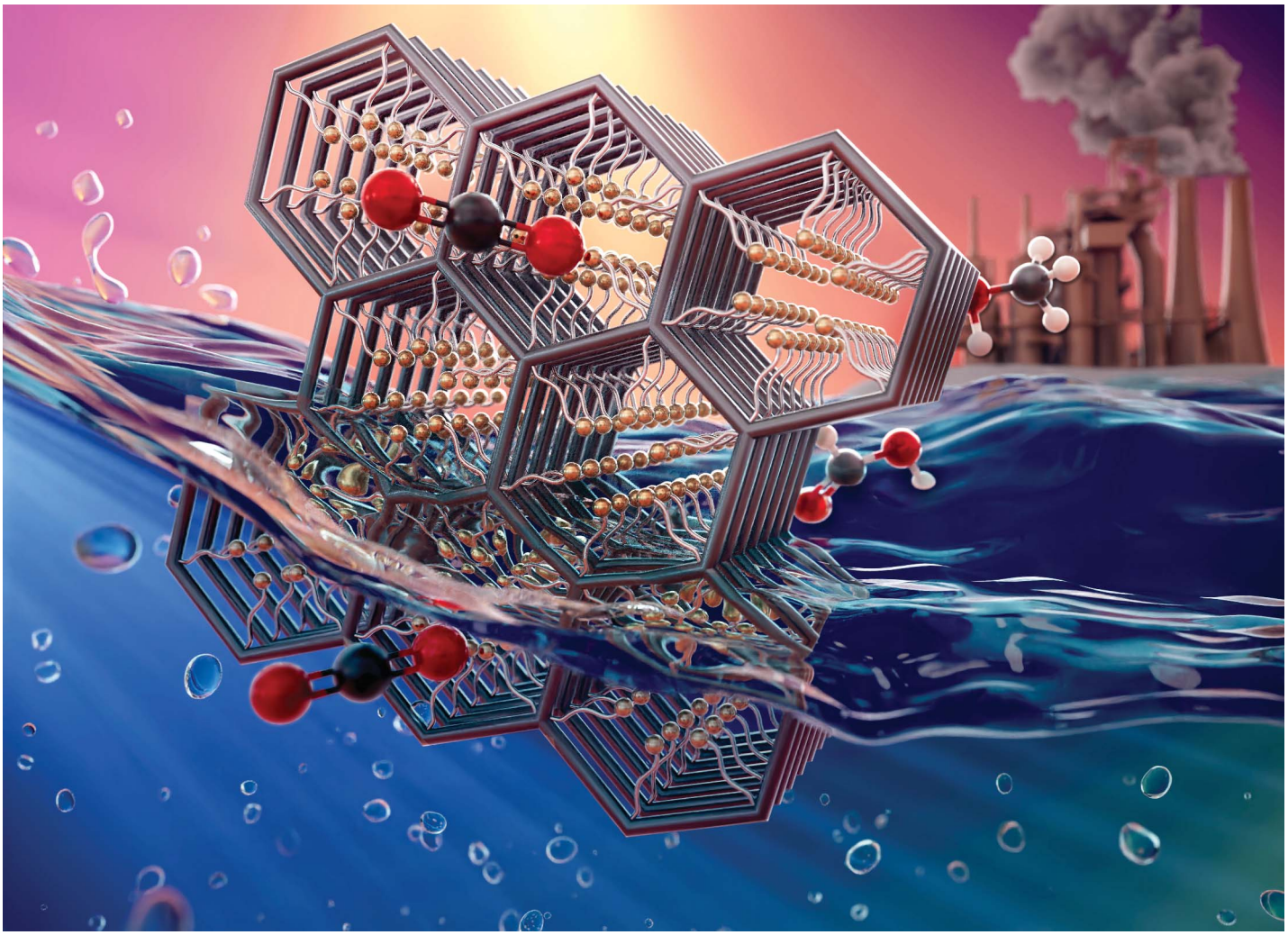

Showcasing research from Professor Leila Negahdar's laboratory, School of Chemistry, University College Dublin, Dublin, Ireland. Art by the team of INMYWORK Studio.

Multifunctionalized zirconium-based MOF as a novel support for dispersed copper: application in CO_2 adsorption and catalytic conversion

A novel multifunctional NU-1000 MOF-Cu material is designed for CO_2 adsorption and catalytic conversion. The copper based catalyst is shown to be active in CO_2 electroreduction and has excellent selectivity towards methanol formation under mild hydrogenation process.

Art by the team of INMYWORK Studio (https://inmywork.com).

As featured in:

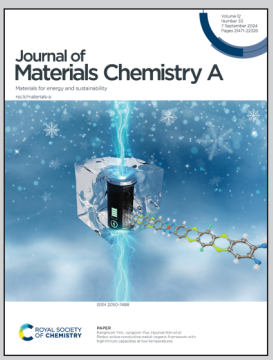

See Concepción Domingo, Leila Negahdar *et al.*, *J. Mater. Chem. A*, 2024, **12**, 21758.

ROYAL SOCIETY OF CHEMISTRY

rsc.li/materials-a

Registered charity number: 207890

Journal of Materials Chemistry A

ROYAL SOCIETY OF CHEMISTRY

PAPER

View Article Online
View Journal | View Issue

Cite this: J. Mater. Chem. A, 2024, 12, 21758

Multifunctionalized zirconium-based MOF as a novel support for dispersed copper: application in CO_2 adsorption and catalytic conversion†

Albert Rosado, [a] Ioana-Maria Popa,[b] Ahmad Abo Markeb, [cd] Javier Moral-Vico,[c] Eva Maria Naughton, [f] Hans-Georg Eckhardt,[f] José A. Ayllón, [e] Ana M. López-Periago, [a] Concepción Domingo *[a] and Leila Negahdar *[f]

CO_2 conversion and utilization for global sustainability is an integral part of greenhouse gases management, typically for the production of fuels and specialty chemicals. Added value products, such as methanol, methane or formate, can be obtained by electrocatalysis and thermocatalysis, the two techniques addressed in this study. The main motivation of this study is to develop a copper based catalyst active in both processes, confronting the main concerns regarding typical metal catalysts related to nanoparticles aggregation and concomitant deactivation. For this, modified NU-1000, a water-stable mesoporous MOF, is used as a platform for the simultaneous coordination–stabilization of copper single atoms and CO_2 adsorption. NU-1000 is synthetized with primary amino groups ($-NH_2$ with affinity for CO_2) by modifying the ligand prior to MOF synthesis, while post-synthetic solvent-assisted ligand incorporation is applied to insert thiol functionalities (–SH with affinity for copper) within the framework. To make the functionalized MOF catalytically active, a Cu^{2+} salt is impregnated into the MOF channels, which is further reduced with H_2 to Cu^+/Cu^0 before performance assessment in CO_2 conversion processes. The as-synthetized and spent catalysts were analysed regarding the structure (X-ray diffraction, infrared), bulk (mass spectrometry) and surface (X-ray photoelectron spectroscopy) composition, morphology (electronic microscopy and energy dispersive spectroscopy) and textural properties (N_2 physisorption). The electrocatalytic reduction of CO_2 was performed in the potential range of −0.8 to −1.8 V, indicating the formation of formic acid. Thermocatalytic experiments were carried out in an economically and energetically sustainable low-

Received 10th May 2024
Accepted 18th July 2024

DOI: 10.1039/d4ta03268c

rsc.li/materials-a

[a]Materials Science Institute of Barcelona, ICMAB-CSIC, Campus UAB s/n, 08193 Bellaterra, Spain. E-mail: conchi@icmab.es
[b]Department of Chemistry, RWTH Aachen University, Aachen 52074, Germany
[c]Department of Chemical, Biological and Environmental Engineering, UAB, Campus UAB s/n, 08193 Bellaterra, Spain
[d]Department of Chemistry, Faculty of Science, Assiut University, Assiut 71516, Egypt
[e]Department of Chemistry, UAB, Campus UAB s/n, 08193 Bellaterra, Spain
[f]School of Chemistry, University College Dublin, Belfield, Dublin 4, Ireland. E-mail: leila.negahdar@ucd.ie

† Electronic supplementary information (ESI) available. See DOI: https://doi.org/10.1039/d4ta03268c

Leila Negahdar

Leila Negahdar received her PhD in Chemistry (Magna Cum Laude) from RWTH Aachen University in 2015 working with Prof. Regina Palkovits on mechanistic study of catalytic conversion of cellulosic biomass to valuable fuels and platform chemicals. After her PhD, she joined group of Prof. Bert Weckhuysen at Utrecht University, working on in situ and operando spectroscopy techniques to understand the catalyst behavior under working conditions. On her return to Germany as postdoctoral research fellow, she started research on electrocatalysis especially gaining knowledge on the mechanism of water oxidation in hydrogen production. In 2019, she moved to Cardiff University/UK catalysis hub working with Professors Richard Catlow and Andrew Beale to study the surface catalysis using central facilities for lasers and synchrotron radiation at Harwell Science and Innovation Campus. She was awarded Marie Skłodowska-Curie individual fellowship based at UCL to work on operando spectroscopy kinetic analysis of catalytic surface reactions. She was appointed as assistant professor in Sustainable Chemistry at UCD in 2022.

pressure (1 MPa) hydrogenation process. Methanol was obtained with 100% selectivity at temperatures up to 280 °C, and a space-time yield of *ca.* 100 mg_{MeOH} g_{cat}^{-1} h^{-1} which overcomes that of commercial CuZnO NPs designed for this purpose.

1 Introduction

During the last century, the world has witnessed a tremendous industrial expansion, concomitant with a dramatic accumulation of greenhouse gases in the atmosphere. The absorption of thermal infrared radiation from the sunlight by these gases is the principal cause of the concerning global warming in the earth surface.[1] Among discharged pollutants by human activity, CO_2 is the most emitted gas, since it is generated as a byproduct in fossil fuels combustion and numerous industrial processes.[2] The increased awareness of the current environmental situation has prompted governments and institutions to establish new policies and restrictions to reduce CO_2 emissions. Procured actions are showing some positive results, although accelerated efforts are still required to meet essential ambitious targets, such as those settled for Europe in the 2030 agenda.[3] For these reasons, investment in the development of advanced technologies to reduce the amount of CO_2 emission from industrial processes is essential, either through its capture or conversion into value-added products, such as plastics, building materials, synthetic fuels or chemicals (*e.g.*, urea, methane, methanol, ethanol, formic acid, acetic acid),[4] thus generating a carbon circular economy. CO_2 capture and separation systems have already been established to an industrial scale, but conversion technologies are still at development stages. Since CO_2 is a thermodynamically stable compound, its conversion requires a catalyst and additional energy input to overcome the reaction activation barrier.[5] The most mature technologies for this purpose are thermocatalytic CO_2 hydrogenation, driven by a combination of temperature and pressure,[6] and electrocatalytic CO_2 reduction, powered by an electrical supply.[7]

The effective thermo or electrocatalytic conversion of CO_2 comprises the use of a catalyst system with active metal sites, frequently dispersed on a support.[8] Among the reported heterogeneous catalytic systems, copper nanoparticles (Cu NPs) have shown great catalytic activity for CO_2 conversion.[9] Indeed, alloys of copper and zinc oxide (Cu/ZnO) NPs are considered as the flagship catalyst in the thermocatalysis of CO and CO_2,[10] while dispersed Cu NPs have been used to produce hydrocarbons and alcohols by electrochemical CO_2 reduction under relatively low overpotentials.[11]

In heterogeneous catalysis, the rational design of the supporting matrix is a decisive point to be considered.[12] The use of a support is necessary to increase the dispersion of the metal surface active centres, by preventing aggregation and sintering of the NPs, as well as to improve the electronic properties of the catalyst. Porous materials, such as oxides, silica, zeolites, carbons and polymers are the most frequently used supports. Recently, metal–organic frameworks (MOFs) have emerged as a novel class of crystalline porous materials with high potential to design energy-intensive processes of gas adsorption and catalysis.[13] The main advantages reside in the unprecedented versatile chemistry of MOFs, which allows adjusting the compositional and textural properties of the framework for each defined purpose.[14] Microporous and mesoporous MOFs have been investigated in the area of catalysis showing promising performance, either as pristine compounds or by forming composites with active metal particles.[15,16] In fact, they are one of the most promising and versatile platforms for fabricating single-site catalysts.[17] Synthetizing water stable MOFs, for instance by combining a strong Lewis base linker (*e.g.*, carboxylate-based) and a strong Lewis acid metal ion (*e.g.*, Zr^{4+}), would certainly widen the range of applications.[18] Examples of those materials are the microporous UiO-66 and the mesoporous NU-1000 phases. NU-1000 is a zirconium-based MOF constituted of tetratopic 1,3,6,8-tetrakis(*p*-benzoic-acid)pyrene (H_4TBAPy) linkers and oxo-Zr_6 $[Zr_6O_{16}H_{16}]^{8+}$ nodes, with a bimodal distribution of unidirectional void channels of diameter 1.2 and 3 nm and a surface area > 2000 m^2 g^{-1}, which has been widely studied in energy and environmental applications, such as photocatalytic and electrocatalytic water splitting, electrocatalytic CO_2 reduction, lithium–sulfur batteries, hydrogen storage, gas adsorption and separation, *etc.*[19]

This study aims to rationally design and synthesize a functionalized NU-1000 MOF that can act as a platform for simultaneous coordination–stabilization of copper single atoms and CO_2 adsorption, and be effective for the conversion of this gas in thermo and electrocatalysis. The NU-1000 MOF was chosen because of its outstanding textural properties, as well as its facility for reticular linker modification and ability of anchoring exogenous metal centres at the metal clusters. Particularly, NU-1000 was synthetized with primary amino groups (–NH_2 with affinity for CO_2), by modifying the ligand prior to the MOF synthesis,[20] while post-synthetic solvent-assisted ligand incorporation (SALI)[21] was applied to insert a free thiol functionality (–SH with affinity for copper) within the framework. This work demonstrates that it is possible to sketch a protocol that allows the incorporation into the NU-1000 of more than one functionality, while maintaining the structural stability of the framework, and, importantly, retaining significant porosity. To make the functionalized MOF catalytically active, a Cu^{2+} salt is impregnated into the MOF channels, which is further reduced with H_2 before performance assessment in CO_2 conversion processes. Comprehensive solid-state characterization of the composite is performed to understand the catalytic behaviour.

The –NH_2 and –SH functionalized NU-1000 was verified as a catalyst platform in electrocatalysis and thermocatalysis processes applied to CO_2 conversion.[22,23] The electrocatalytic activity was measured using working electrodes consisting of modified NU-1000/Cu grown as a film on a conducting substrate selected from either fluorine-doped tin oxide (FTO) conducting glass or reduced graphene oxide (rGO). Furthermore, the thermocatalytic activity of the material was tested in an economically attractive and energetically sustainable low pressure (1

MPa) hydrogenation process.[24] The developed material is shown to have promising catalytic activity.

2 Materials and methods

2.1. Materials

The employed reactants and solvents for MOFs synthesis, post-synthetic modification and characterization were 1,3,6,8-tetrakis(*p*-benzoic-acid)pyrene (H_4TBAPy, BLDpharm), zirconium(IV) chloride ($ZrCl_4$, abcr), benzoic acid (BA, Fluka), diethyl formamide (DEF, abcr), dimethylformamide (DMF, abcr), hydrochloric acid (HCl, abcr), acetone (abcr), dichloromethane (DCM, abcr), 3-mercaptopropionic acid (PrSH, abcr), copper formate hydrate ($Cu(For)_2$, abcr), methanol (MeOH, abcr), hydrofluoric acid (HF, Fluka) and deuterated dimethyl sulfoxide (DMSO-d_6, abcr). Fluorine doped tin oxide (FTO) glass was provided by Merck. rGO support was prepared from a graphene oxide dispersion in water (GO, 0.004 wt%) provided by Graphenea Inc., after thermal reduction with ascorbic acid (HAsc, Fluka), solvent-exchange with absolute ethanol (EtOH, abcr) and supercritical CO_2 ($scCO_2$) drying. The CO_2, H_2, H_2 : Ar (5 : 95 v%) and CO_2 : H_2 (1 : 3 mole ratio) gases were delivered by Carburos Metálicos S.A. The electrolyte solutions were prepared with potassium hydrogencarbonate ($KHCO_3$) and sodium perchlorate ($NaClO_4$) purchased from Fisher Sci. and MilliQ water obtained from Merck Q-POD.

2.2. Synthetic procedure

2.2.1. Synthesis of NU-1000, NU-1000-NH_2 and NU-1000-NH_2/PrSH. NU-1000 and NU-1000-NH_2 were synthetized following a reported procedure,[25] using as linkers H_4TBAPy and H_4TBAPy–NH_2, respectively. While H_4TBAPy is a commercial reagent, H_4TBAPy–NH_2 was synthetized according to an established protocol,[20] which is summarized in the ESI.† The synthesis of these MOFs started by sonicating 70 mg (0.30 mmol) of $ZrCl_4$ and 2700 mg (22.1 mmol) of BA in a 6-dram vial filled with 8 mL of DEF. The solution was heated at 80 °C for 1 h and cooled down. Then, 40 mg (0.06 mmol) of H_4TBAPy or 45 mg (0.06 mmol) of H_4TBAPy–NH_2 were added to the vial, dispersed by 20 min sonication and solvothermally treated at 110 °C for 48 h. Once cooled again, the obtained precipitate was solvent-exchanged with fresh DMF three times. Then, the MOF was treated with a mixture of DMF (12 mL) and HCl 6 M (0.7 mL) at 100 °C for 24 h to remove the pendant benzoate ancillary ligands. The obtained crystals were washed thrice with DMF and acetone by solvent exchange, and dried under vacuum. NU-1000-NH_2 was post-synthetically modified with –PrSH following the SALI protocol reported for NU-1000 for diverse carboxylic acids.[21] In this work, 50 mg (*ca.* 0.02 mmol) of NU-1000-NH_2 were dispersed in a mixture containing 20 μL (0.22 mmol) of PrSH and 3 mL of DMF. The closed vial was heated at 60 °C during 24 h with occasional hand-shaking. After this time, the crystals were filtered and washed consecutively with fresh DMF, acetone and DCM. The product was activated under vacuum (700 Pa) at 120 °C for 4 h. Orangish NU-1000-NH_2/PrSH microcrystals were recovered (Fig. 1).

2.2.2. Copper impregnation and reduction: NU-1000-NH_2/PrS–Cu. 28 mg (*ca.* 0.01 mmol) of NU-1000-NH_2/PrSH crystals were impregnated with 10 mg (0.06 mmol) of $Cu(For)_2$ dissolved in 10 mL of MeOH. The vial containing the mixture was left to rest for 2 days. After this time, the blue colour in the solution disappeared and the MOF orangish crystals turned greenish (Fig. 1). The product was washed four times with fresh MeOH prior to vacuum drying to afford the NU-1000-NH_2/PrSH–$Cu(For)_2$ sample. This product was thermally reduced under a flow of diluted H_2 in Ar (150 mL min^{-1}) in a tubular oven at

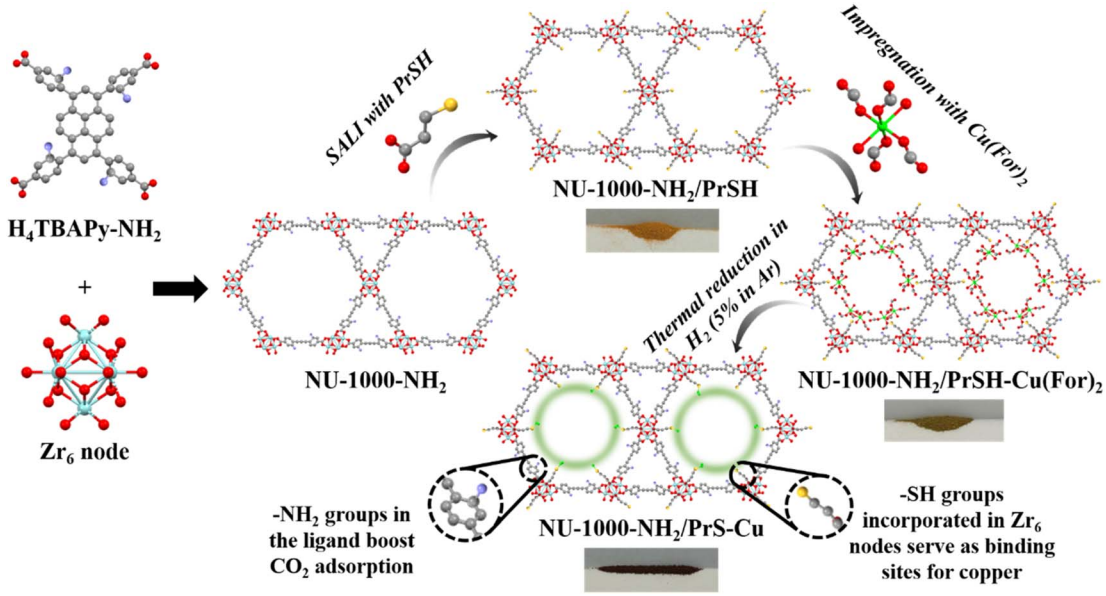

Fig. 1 Schematic representation of the followed steps to synthesize NU-1000-NH_2/PrSH–Cu, emphasizing in the purpose of the installed functionalities and including the color variation of the powder.

160 °C for 2 h. The obtained brownish NU-1000-NH_2/PrS–Cu sample was kept in a desiccator for subsequent characterization (Fig. 1).

2.3. Electrocatalytic experiments

The working electrodes for these experiments were assembled by *in situ* growth of NU-1000-NH_2 on a support of either rectangular cut pieces of commercial FTO conducting glass (1.60 × 1.40 cm) or home-made rGO rounded films (1.2 cm diameter). For rGO supports preparation, first a GO dispersion in water was reduced with 160 mg (0.91 mmol) of HAsc at 95 °C for 1 h. The resulting hydrogel was thoroughly washed with distilled water and solvent-exchanged with absolute EtOH to obtain an alcogel that was dried under $scCO_2$ at 20 MPa and 60 °C, resulting in a monolith of rGO aerogel.[26] Finally, the rGO monolith was pressed at 2.5 tons per cm^2 to yield rGO disk-shape films (Fig. 2). To grow the catalytic MOF on the supports, similar steps to the above described protocol to synthetize the powder were followed. Thus, NU-1000-NH_2 crystals were straightforwardly grown on conducting FTO plates or rGO disks (Fig. 2). The supports were perpendicularly held with the aid of a PTFE tape and immersed in the synthetic medium used to prepare the MOF. The recovered NU-1000-NH_2@support composites were post-synthetically modified with PrSH to yield the NU-1000-NH_2/PrSH@support samples. Finally, the systems were impregnated with $Cu(For)_2$ in MeOH to afford the NU-1000-NH_2/PrSH–$Cu(For)_2$@support precursors and transformed by soft H_2 thermal reduction to NU-1000-NH_2/PrS–Cu@support electrodes.

The electrocatalytic experiments were performed in a one-pot home-made cell with anodic and cathodic spaces (described in the ESI†). The cell was filled with either $NaClO_4$ or $KHCO_3$ electrolyte. A Pt sheet, Ag/AgCl and NU-1000-NH_2/PrS–Cu@support were used as the anodic, reference and working cathodic electrodes, respectively. Prior to the electrocatalytic tests, a short treatment at −0.6 V *vs.* the reference hydrogen electrode (RHE) was applied to the sample to afford completely reduced copper. After this pre-treatment, cyclic voltammetry (CV) scans were performed at different scan rates (60, 80, 100, 250 and 300 mV s^{-1}) to estimate the electrochemical surface area (ECSA) through the calculation of the double layer capacitance (C_{dl}) in a non-faradaic region.[27] Note that C_{dl} is directly proportional to the ECSA. The electrochemical testing was then straightforwardly conducted at −0.4, −0.7, −0.8, −1.0, −1.2, −1.4, −1.6 and −1.8 V *vs.* RHE as a chronoamperometric measurement for 1 h while keeping the CO_2 bubbling in the cathodic space. Gas and liquid aliquots were collected every 20 min. Gas samples were analysed in a Varian GC-450 gas chromatograph, equipped with a methaniser, TCD and FID detectors. Liquid samples were analysed by HPLC (Agilent 1200 reverse phase with an Automated Liquid Sampler (Agilent ALS G1329A)).

2.4. Thermocatalytic experiments

20 mg of NU-1000-NH_2/PrS–Cu powder were dispersed in glass wool, placed inside a fixed-bed tubular column (0.45 × 9 cm, ∅ × l) and subjected to *in situ* reduction with a flow of H_2 (20 mL min^{-1}) at 180 °C for 2 h. A home-made Process Integral Development Engineered & Tech. equipment was used for catalytic activity measurements (described in the ESI†). After switching the flow from pure H_2 to a mixture of CO_2 : H_2, the pressure was set at 1 MPa, while the gas flow rate was fixed at 10 mL min^{-1}. Ejected products were determined in the temperature range of 180–280 °C every 20 min. MeOH was measured using a Shimadzu GC-2010 gas chromatograph. The presence of gases (CO_2, CO, *etc.*) was evaluated using an Agilent Tech. 7890B gas chromatograph. MeOH space-time yield (STY_{MeOH}) was estimated based on catalyst weight.

2.5. Characterization techniques

The crystalline structure of the products was characterized by powder X-ray diffraction (PXRD) in a Bruker D8 Advance with Cu Kα incident radiation. The molecular structure was evaluated by Fourier transform infrared (FTIR) spectroscopy (Jasco 4700 Spectrophotometer) using the attenuated total reflection (ATR) accessory. Proton nuclear magnetic resonance (^{1}H-NMR, Bruker Advance NEO 300 MHz) was used to characterize the organic products obtained during H_4TBAPy–NH_2 synthesis, and to quantify the content of PrSH after MOF digestion in HF and

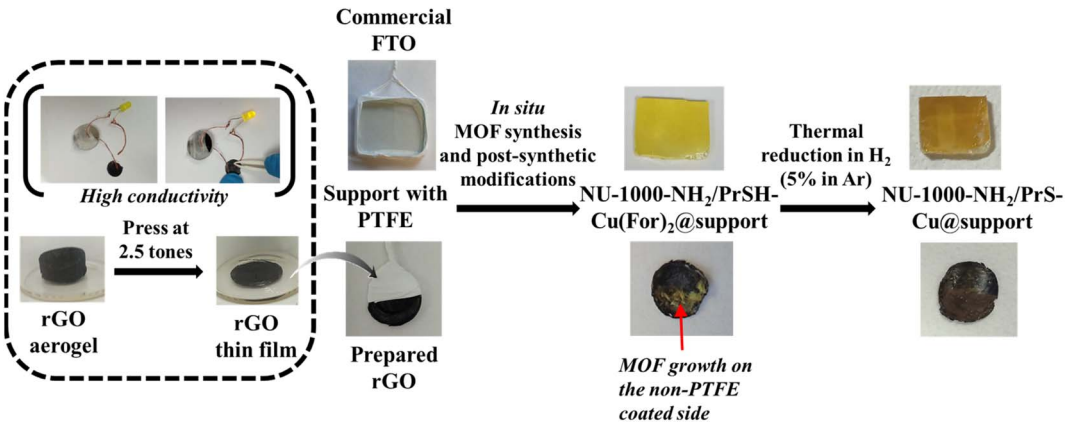

Fig. 2 Schematic representation of NU-1000-NH_2/PrS–Cu@support preparation.

further dissolution in DMSO-d_6.[28] Sample morphology and size were examined using a scanning electron microscope (SEM, Quanta FEI 200), with coupled energy-dispersive spectroscopy (EDS, using an Inca 250 SSD XMax20 detector) to evaluate atomic dispersion, and a transmission electron microscope (TEM, JEOL 1210). Samples characterized by SEM were coated with Pd/C prior to the analysis, while those used in EDS or TEM were not. Inductively coupled plasma mass spectrometry (ICP-MS, 7700x Agilent) was used to ascertain the Zr : Cu ratio. Samples were digested with a mixture of hydrochloric acid, nitric acid and MilliQ water (3 : 1 : 2 v/v) in a microwave oven at 200 °C previous to the analysis. An X-ray photoelectron spectrophotometer (XPS, KRATOS AXIS Ultra DLD spectrometer equipped with a monochromatic Al Kα source (1486.6 eV, 150 W)) was utilized to evaluate the electronic state of nitrogen (N_{1s}), sulfur (S_{2p}) and copper (Cu_{2p}) in the samples. XPS data was analysed by AAnalyzer software. The thermal stability of the products was examined by thermogravimetric analysis (TGA, Q500) under a flow of H_2 diluted in Ar (40 mL min^{-1}) with a ramp of 5 °C min^{-1}. For the characterization of the textural properties, N_2 adsorption–desorption isotherms were recorded at −196 °C in a Micromeritics ASAP 2020 equipment. Samples were previously activated at 120 °C under high vacuum (15 Pa) during 20 h. The apparent specific surface area was calculated by applying the Brunauer–Emmet–Teller (BET), while the pore volume and pore size distribution was estimated by the Barrett–Joyner–Halenda (BJH) and Dubinin–Astakhov (D–A) methods.[29] Using the same equipment and activation conditions, measurements of CO_2 adsorption were performed at temperatures (T) of 0, 25 and 40 °C and pressures (p) from vacuum to 100 kPa. From these data, the CO_2 enthalpy of adsorption (Q_{st}) was determined at different levels of surface occupancy (n) by applying the Clausius–Clapeyron equation $Q_{st}(n) = -R\ln(p_2/p_1)(T_1T_2/(T_2 - T_1))$.

3 Results and discussions

3.1. Structure and composition of the catalyst

NU-1000 was first modified with amino (–NH_2) and thiol (–PrSH) groups, installed in the linker and metal nodes, respectively. Subsequently, Cu(For)$_2$ was impregnated into the MOF pores. Finally, the system was reduced with H_2 to obtain the active catalyst NU-1000-NH_2/PrS–Cu, tested for the conversion of CO_2. Each product, obtained in a stepwise rational material design, was thoroughly characterized by solid state techniques to evaluate the effectiveness of the performed modifications.

3.1.1. Addition of –NH_2 for CO_2 adsorption. The first synthetic step in the design of the catalyst, was the addition of primary arylamines as a part of the NU-1000 framework. NU-1000-NH_2 crystals were recovered as aggregated particles with a morphology of thin elongated hexagonal prisms of 5–15 μm average length and 3–4 μm average diameter (Fig. S8†). The recorded PXRD for the crystallized NU-1000-NH_2 displayed the same pattern as NU-1000, with the most intense band at 2θ = 2.6° (Fig. S9†). The ATR-FTIR spectrum shows the typical NU-1000 bands,[30] together with those assigned to added amino groups, such as aromatic –NH_2 Fermi resonance and N–H bending at *ca.* 3000 and 1650 cm^{-1}, respectively (Fig. S10†). NU-1000 is an archetypical MOF characterized by its highly porous crystalline architecture, but with a framework displaying low CO_2 affinity. In different works, CO_2 uptake has been improved by post-synthetic inclusion in the pores of certain functionalities, *e.g.*, perfluoroalkenes or compounds with amino groups.[31–34] However, this method results in important reduction of the effective pore volume, which would hinder the incorporation of catalytically active entities within the structure and, further, prevent a proper diffusion of reactants and products throughout the framework. Hence, to develop an efficient system for CO_2 conversion, it is of vital importance to endow the MOF with energetically favourable sites for CO_2 adsorption, but preserving the empty pore volume to a large extent. In this work, the inclusion of primary amino groups in the NU-1000 framework as part of the MOF linker (H_4TBAPy–NH_2) was pointed to address both key factors. To evaluate the influence of the installed –NH_2 functionalities on the porosity of the system, N_2 isotherms of pristine and amino functionalized MOF were recorded and compared. The two pairs of adsorption–desorption curves overlapped in the graph (Fig. 3a), denoting that the NU-1000 porous framework was preserved in NU-1000-NH_2. Indeed, the addition of –NH_2 functionalities did not significantly modify the surface area and pore volume of NU-1000-NH_2 when compared to NU-1000, just decreasing from 2230 to 2140 $m^2\ g^{-1}$ and from 1.70 to 1.50 $cm^3\ g^{-1}$ BJH (1.01 to 0.82 $cm^3\ g^{-1}$ D–A), respectively, thus leaving enough space for subsequent post-synthetic modification and catalytic reactions. The effect of the installed primary amino groups on CO_2 uptake was assessed by measuring the adsorption isotherm at 0 °C up to saturation pressure for net and functionalized MOF. Remarkably, the CO_2 adsorption capacity increased from 3.25 mmol g^{-1} in pristine NU-1000 to 5.36 mmol g^{-1} in NU-1000-NH_2 at 100 kPa (Fig. 3b), denoting that these primary amino groups indeed play the role of Lewis bases for enhancing CO_2 adsorption.[35]

3.1.2. Addition of –SH binding sites for copper fixation. The second step in the preparation of the catalyst consisted in the post-synthetic modification of NU-1000-NH_2 with –PrSH, which is aimed to provide the system with potential binding sites for individual copper units, thus enabling the formation of a single-atom catalyst. The –PrSH ligands were successfully integrated in the NU-1000-NH_2 framework through the coordination of the carboxylate group with the exposed vertexes of the Zr_6O_8 cluster located at the nodes of the MOF framework. According to ^{1}H-NMR quantitative analysis (see ESI† for the description of the method), the four available positions in each Zr_6O_8 cluster were successfully occupied by –PrSH, thus giving a Zr : S atomic ratio of 6 : 4 (Fig. S12†). The PXRD pattern recorded for NU-1000-NH_2/PrSH matches that of the NU-1000 phase, indicating that –PrSH functionalization did not provoke significant framework distortion (Fig. S9†). The ATR-FTIR spectrum did not account for additional signals with respect to NU-1000-NH_2, which is attributed to the weak intensity of –SH infrared vibrations as well as to the overlapping of the aliphatic and carboxylate bands with the ones of NU-1000-NH_2 (Fig. S10†). The homogeneous distribution of sulfur in one crystal of NU-1000-NH_2/PrSH was confirmed by EDS

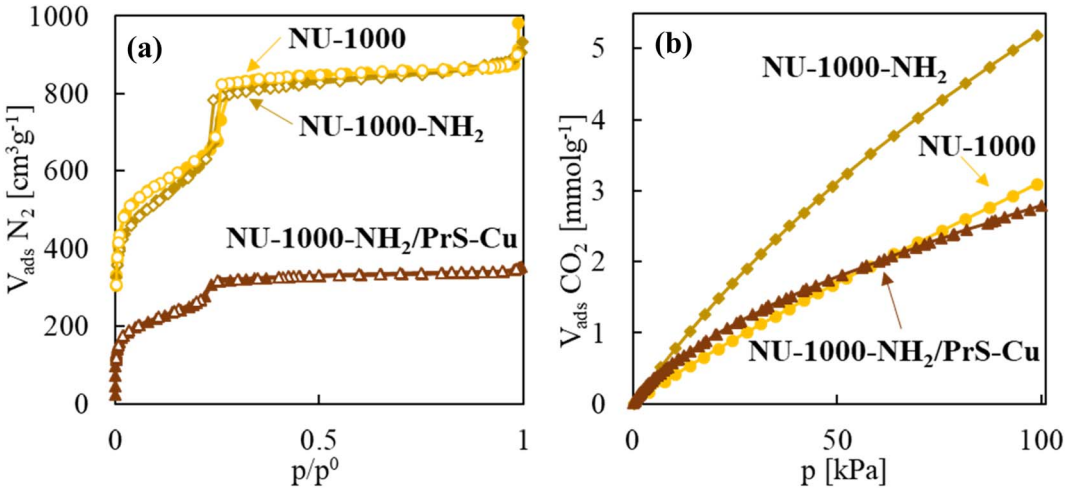

Fig. 3 Adsorption behavior: (a) N_2 adsorption–desorption isotherms at −196 °C and (b) CO_2 adsorption isotherms at 0 °C of the studied samples compared to pristine NU-1000.

mapping in a non-metalized sample (Fig. S13†). Importantly, it was demonstrated that the applied SALI method[21] can be used to modify the Zr-clusters even in the vicinity of amino functionalities.

3.1.3. Impregnation with $Cu(For)_2$ and reduction. In the last synthetic step, a copper salt was incorporated into the open volume of the synthetized NU-1000-NH_2/PrSH framework as the precursor to further afford the active catalyst by thermal reduction. $Cu(For)_2$ was chosen for this purpose, because it can be reduced to copper metal at relatively low temperatures (<200 °C),[36] thus avoiding any thermal damage of the functionalized MOF framework. The incorporation of blue $Cu(For)_2$ to the MOF led to visual differences in the colour of the crystals, shifting from orange in the pristine NU-1000-NH_2/PrSH to green in the loaded NU-1000-NH_2/PrSH–$Cu(For)_2$ (Fig. 1). The amount of impregnated copper precursor was analysed by ICP-MS, giving a ratio Zr : Cu of 6 : 4.6. The large amount of incorporated $Cu(For)_2$ (*ca.* 15 wt%) is justified on the basis of the added functionalities on the NU-1000 framework, which serve as anchoring points for the impregnated copper salt, especially, the exposed thiol groups, according to the hard and soft (Lewis) acids and bases principle. $Cu(For)_2$ addition did not entail any significant variation in the PXRD pattern, in which the $Cu(For)_2$ most intense peaks, located at 2θ *ca.* 17 and 29°, were not present (Fig. S9†). The EDS spectrum obtained by line scan in an individual crystal indicated that added Cu^{2+} was homogeneously distributed along the MOF, similarly to zirconium (Fig. 4a and b). The interaction of loaded $Cu(For)_2$ with the pendant functionalities in the MOF was further analysed by recording the XPS spectrum of the NU-1000-NH_2/PrSH–$Cu(For)_2$ sample (Fig. 4e–g(I)). The band associated to N_{1s} could be fitted with a singlet centred at a binding energy of 400.0 eV, characteristic of primary amino groups, with no sign of Cu–N bond (Fig. 4e(I)).[37] As well, the band associated to S_{2p} could be fitted with typical unbounded thiol doublet, displaying peaks at binding energies of 163.5 ($S_{2p_{3/2}}$) and 164.7 ($S_{2p_{1/2}}$) eV and an area ratio of 2 : 1 (Fig. 4f(I)).[38] Regarding the electronic configuration of copper, the Cu_{2p} spectrum displayed the typical peaks of divalent copper at binding energies of 934.5 ($Cu_{2p_{3/2}}$) and 954.4 ($Cu_{2p_{1/2}}$) eV, with their corresponding satellites at *ca.* 943 and 963 eV, while only a low intensity signal at 932.8 eV featured the presence of a small percentage of Cu^+/Cu^0 (Fig. 4g(I)).[39,40] Actually, the recorded Cu_{2p} spectrum was exactly the same as the one for net $Cu(For)_2$.[41] These results together indicate that $Cu(For)_2$ would established only low-energy electrostatic interactions in the MOF with the pendant –NH_2 or –PrSH functionalities. Taking into account that the ratios Zr : SH and Zr : Cu were estimated as 6 : 4 and 6 : 4.6 by ^{1}H-NMR and ICP-MS, respectively, in first instance it is rationalized that all thiol, and only few amino, sites were occupied by $Cu(For)_2$.

Catalytically active copper sites are generated in the precursor NU-1000-NH_2/PrSH–$Cu(For)_2$ by thermal reduction at 160 °C with H_2 diluted in Ar. This working temperature was selected after examining the TGA curve of NU-1000-NH_2/PrSH–$Cu(For)_2$ and comparing with the ones of $Cu(For)_2$ and NU-1000-NH_2/PrSH, all recorded under a similar reducing atmosphere (Fig. S14†). In both NU-1000-NH_2/PrSH and NU-1000-NH_2/PrSH–$Cu(For)_2$, a weight decay was observed in the 250–400 °C temperature interval associated with the loss of –NH_2 and –PrSH pendant functionalities, being the NU-1000 framework skeleton thermally stable up to *ca.* 450 °C. The NU-1000-NH_2/PrSH–$Cu(For)_2$ sample has an extra weight drop starting at *ca.* 150 °C, attributed to the reduction of $Cu(For)_2$ and the subsequent release of CO_2 and H_2. The selected thermal treatment caused a colour change in the recovered sample, designated as NU-1000-NH_2/PrS–Cu, from green to brown (Fig. 1), which is ascribed to copper reduction. To ascertain the electronic configuration of copper after sample reduction, the XPS spectrum of NU-1000-NH_2/PrS–Cu was analysed in the Cu_{2p} region (Fig. 4g(II)). The peaks previously associated to Cu^{2+} in NU-1000-NH_2/PrSH–$Cu(For)_2$ shifted to low binding energies in the reduced product (933.0 eV in $Cu_{2p_{3/2}}$ and 952.9 eV in $Cu_{2p_{1/2}}$), with barely visible Cu^{2+} satellites, indicating the almost total reduction of $Cu(For)_2$ to Cu^+/Cu^0.[39,40] In the N_{1s} spectrum, no significant differences between non-reduced and reduced samples were

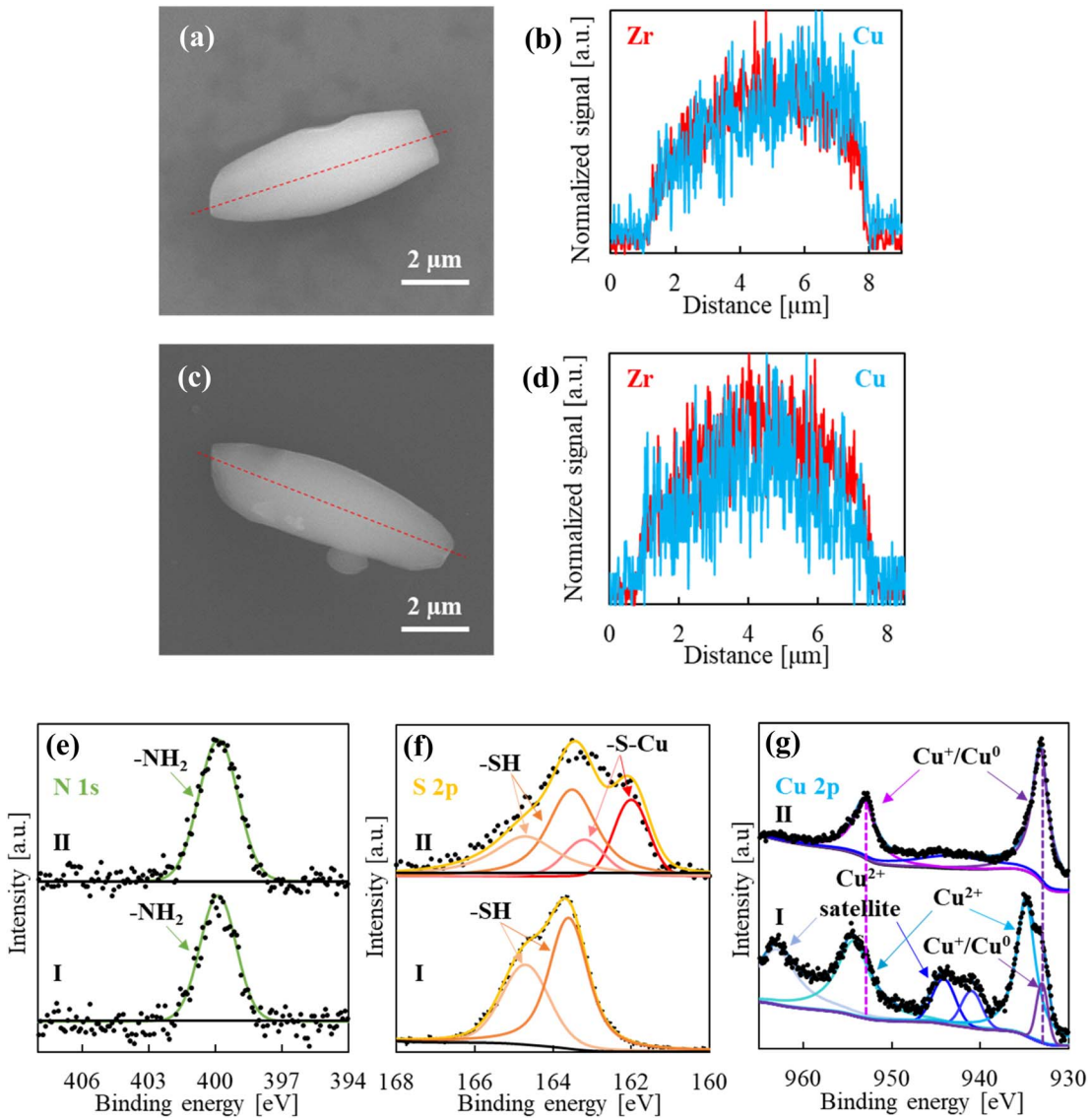

Fig. 4 Characterization before and after thermal reduction: SEM images and Zr *vs.* Cu EDS line scans of (a and b) NU-1000-NH_2/PrSH–Cu(For)$_2$ and (c and d) NU-1000-NH_2/PrS–Cu, respectively; and XPS spectra of (I) NU-1000-NH_2/PrSH–Cu(For)$_2$ and (II) NU-1000-NH_2/PrS–Cu in the (e) N_{1s}, (f) S_{2p} and (g) Cu_{2p} regions, displaying the respective deconvoluted peaks.

found, denoting that the primary amino groups remained unaltered and not bonded to Cu^+/Cu^0 (Fig. 4e(II)).[37] In contrast, an additional doublet, with peaks at binding energies of 161.9 and 163.1 eV, could be fitted in the S_{2p} region (Fig. 4f(II)), associated with the formation of metal-thiolate [–S–Cu^+] bonds.[42] According to the area under the peaks, the formation of thiolate bonds accounts for *ca.* 45% of the total sulfur.

The recovered NU-1000-NH_2/PrS–Cu showed similar morphology and size to the parent NU-1000-NH_2 (Fig. 5a), with no sign of thermal or chemical damage, as confirmed by PXRD (Fig. S9†). It is worth to mention that the typical metallic copper crystals bands at $2\theta = 43.1$ and 50.3° were not depicted in the pattern, indicating that the reduction of Cu(For)$_2$ did not trigger the growth of large Cu NPs (Fig. S15†). Besides, no trace of these NPs deposited on the surface of NU-1000-NH_2/PrS–Cu was observed in the TEM images (Fig. 5b and c). As well, EDS line scan performed in this sample indicates that the homogenous distribution of copper found previously for NU-1000-NH_2/PrSH–Cu(For)$_2$ was maintained after reduction (Fig. 4c and d). Taken these results together, it can be concluded that the added –PrSH functionalities in NU-1000-NH_2/PrS–Cu prevented the migration of copper atoms from the cavities to the outer surface of the MOF during the thermal reduction process, thus avoiding the previously reported drawback of copper aggregation into NPs.[23]

N_2 physisorption analysis exhibits noteworthy values of surface area and pore volume in NU-1000-NH_2/PrS–Cu, in the order of 1130 $m^2\ g^{-1}$ and 0.55 $cm^3\ g^{-1}$ BJH (0.28 $cm^3\ g^{-1}$ D–A), respectively (Fig. 3a and S16 in the ESI† for pore size distribution), which is highly relevant for its further application in catalysis. Even for the NU-1000-NH_2/PrS–Cu product the textural properties were reduced to approximately half of that of NU-1000, the measured CO_2 adsorption at saturation pressure

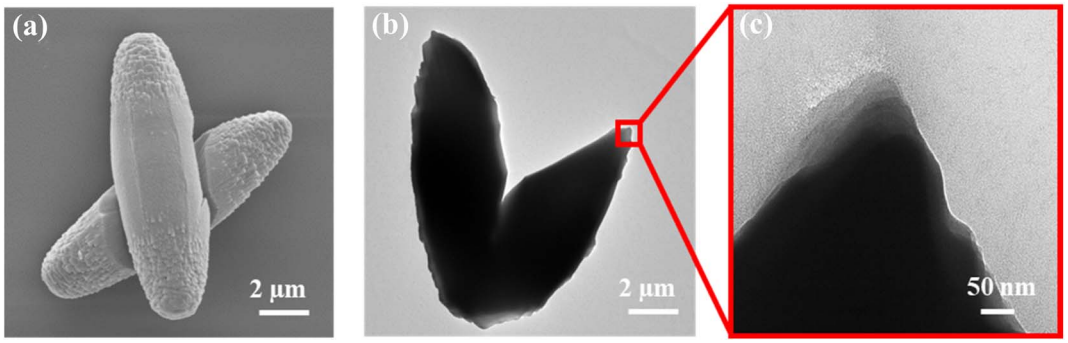

Fig. 5 Microscopic characterization of NU-1000-NH_2/PrS–Cu particles: (a) SEM and (b and c) TEM micrographs.

and 0 °C was similar to that of the pristine MOF, with a value of *ca.* 3.00 mmol g^{-1} (Fig. 3b). For this sample, the isosteric enthalpy of adsorption (Q_{st}) is used as a key parameter to evaluate the advantages of adding –NH_2 functionalities in CO_2 adsorption. For NU-1000, the calculated $-Q_{st}$ values were nearly constant at all the studied surface coverages, with values of 16–18 J $mmol^{-1}$ (Fig. S17†). However, for NU-1000-NH_2/PrS–Cu this energy parameter notably incremented, especially, at low degree of surface occupancy with values close to 30 J $mmol^{-1}$, which is attributed to the adsorption of CO_2 in energetically favourable –NH_2 sites. At higher adsorption values, $-Q_{st}$ values are stabilized at 21–23 J $mmol^{-1}$. Although all these quantities are in the range of physisorption, the CO_2 adsorption enthalpy was notably higher for the MOF involving amino functionalities than for net NU-1000, denoting increased affinity of NU-1000-NH_2/PrS–Cu for CO_2.

3.2. Electrocatalytic reduction of CO_2

High electrical conductivity is rare in MOFs, yet, when present, promising performance in electrocatalytic applications can be envisaged.[43] NU-1000 is known as an insulating material, with a conductivity of 9.1×10^{-12} S cm^{-1}, which does not contain well-defined crystallographic pathways enabling band-like charge transport. Efforts undertaken to increase conductivity in NU-1000 include modifications to preclude direct orbital overlapping and post-processing by host–guest interactions.[44,45] In this study, to measure the electrocatalytic activity of the designed MOF, with a NU-1000 modified linker and host–copper electronic interactions, crystals were grown on a conductive support, either FTO or rGO (Fig. 2). NU-1000-NH_2/PrS–Cu was successfully grown on the chosen supports following the method described in section 2.3. In the PXRD patterns of NU-1000-NH_2/PrS–Cu@FTO and @rGO samples, the most intense peaks of NU-1000 could be identified (Fig. S18†). Further, SEM images showed that NU-1000-NH_2/PrS–Cu small microcrystals with the hexagonal morphology, especially on FTO, were deposited with a random orientation, forming a monolayer covering most of the surface (Fig. 6). Finally, EDS mapping of the composites denoted that copper resides just on the areas where MOF microcrystals were present (Fig. S19†).

First, tests were performed to assure the chemical inertness of the used electrode supports in the selected electrolyte, *i.e.*, $KHCO_3$ and $NaClO_4$, particularly important for FTO substrate that can experience reductive corrosion in either alkaline or acidic media at certain applied voltages, involving the electrochemical reduction of SnO_2 to Sn^0.[46] In the system used in this work, and applying a potential of −0.7 V *vs.* RHE for 10 min, the surface layer of bare FTO darkened due to tin reduction in $NaClO_4$, while it remained stable in $KHCO_3$. Hence, for further experiments, the 0.1 M $KHCO_3$ buffered electrolyte was preferred, since the presence of protons in the acidic solution induced tin reduction even under mild cathodic potentials. This observation was opposite to the behaviour described in a previous work for a non-modified NU-1000/Cu@FTO catalyst, for which best results were obtained with the slightly acidic $NaClO_4$ electrolyte.[23] Prior to sample testing, NU-1000-NH_2/PrS–Cu@FTO was subjected to a short electrochemical treatment at −0.6 V *vs.* RHE to reduce any copper possibly reoxidized during sample manipulation. The effectiveness of this pre-treatment was demonstrated by comparing the CV scan of the sample before and after, the later displaying two more intense sets of Cu-redox peaks (Fig. S20a†). In the NU-1000-NH_2/PrS–Cu@FTO tests, run at −0.4 and −0.7 V *vs.* RHE, neither gaseous nor liquid products were detected in the electrochemical experiments. In contrast, the aliquots collected from the reaction at −0.8 V *vs.* RHE displayed bands corresponding to CO and H_2 in the GC analysis. Nevertheless, at the end of the reaction, it was observed that the working area in the FTO support became darker at this potential, with no sign of MOF particles on the surface (Fig. S21†). Hence, this potential again caused damage to the FTO layer during testing. Actually, the CV scan performed for the electrocatalytically treated sample showed a single set of redox peaks at noticeably different potentials (Fig. S20b†) with respect to the ones assigned to Cu^0 redox peaks (Fig. S20a†), but matching those associated with Sn^0.[47] Similar curves were obtained for bare FTO treated at −0.8 V *vs.* RHE (Fig. S20b†). In light of these results, FTO proved not to be an appropriate support to study the electrocatalytic activity of synthetized NU-1000-NH_2/PrS–Cu, as the limited stability of the support does not allow to work at cathodic potentials high enough (>0.7 *vs.* RHE) to make the designed MOF electrocatalytically active.

To further explore the electrocatalytic capacities of the developed MOF at high potentials, a chemically stable rGO support was taken into consideration.[48] A conductive rGO thin

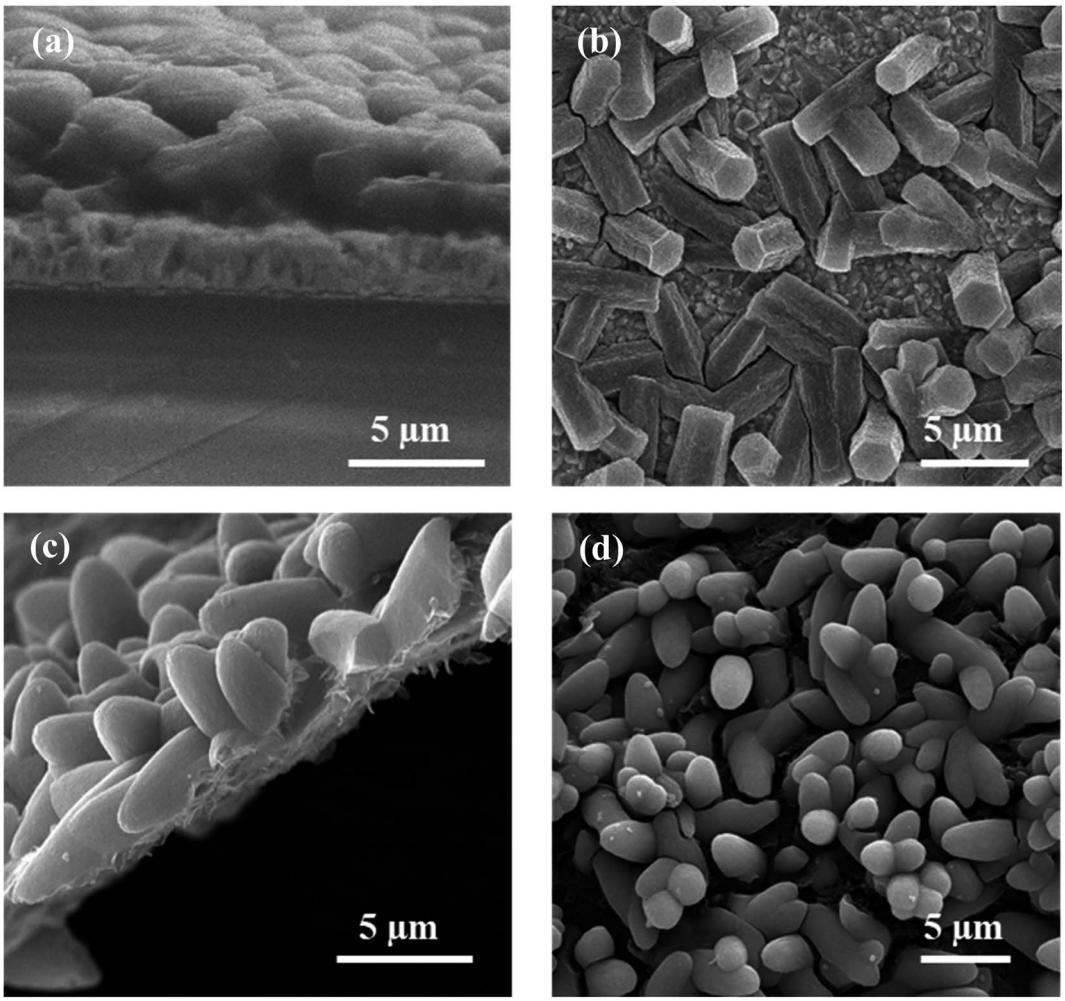

Fig. 6 SEM micrographs of the samples tested for electrocatalysis: (a and b) NU-1000-NH_2/PrS–Cu@FTO and (c and d) NU-1000-NH_2/PrS–Cu@rGO taken from different angles.

film was thus prepared, with an optimal resistance (*ca.* 20 Ω) to ensure adequate charge transfer to the supported MOF. In this case, the CV scan recorded for both bare rGO support and NU-1000-NH_2/PrS–Cu@rGO displayed a similar curve, with no sign of the Cu-redox peaks observed in the NU-1000-NH_2/PrS–Cu@FTO sample, not even after the electrochemical treatment at −0.6 V *vs.* RHE (Fig. S22†). Regardless, this is attributed to the large currents displayed by rGO which most likely overlaps the Cu-redox signals. The bare rGO support was submitted to electrocatalytic tests at a potential as high as −1.2 V *vs.* RHE in 0.1 M $KHCO_3$ electrolyte, showing no apparent structural or chemical modification. At this applied voltage, the production of a certain amount of H_2 from bare rGO could be detected by GC. It has been previously reported that the defects generated in the rGO surface upon reduction can serve as catalytic sites for electrochemical hydrogenation processes.[49] The ECSA of NU-1000-NH_2/PrS–Cu@rGO was estimated by determining the C_{dl} (Fig. S23†).[27] The calculated C_{dl} value was in the order of 0.06 mF cm^{-2}, which is significantly lower than other reported values for Cu-based hybrid materials.[50] However, this may be explained through the large currents displayed by the rGO, which likely cover the CV response of the actual NU-1000-NH_2/PrS–Cu material, as mentioned above. Instead, the measured C_{dl} would describe the rGO substrate more accurately than the electrocatalyst of interest. Testing NU-1000-NH_2/PrS–Cu@rGO as the working electrode in the interval of −0.8 to −1.8 V under similar experimental conditions also resulted in the production of H_2, in a larger extent than for bare rGO. Additionally, according to HPLC results, formic acid could be detected in the liquid phase (Fig. S24†). However, no CO signal could be identified in the GC analysis. CO is recognized as the main intermediate in the electrochemical reduction of CO_2, as starting point to build more complex compounds.[51] Hence, the electrocatalytic synthesis of any CO_2-derived product is typically accompanied by the generation of a certain amount of CO.[50] The mechanism for the conversion of CO_2 into formic acid is still not fully understood and several possible pathways have been proposed.[52] Although in theory formic acid can be straightforwardly produced without the presence of side products, most of the reported routes contemplate the production of CO and H_2O from secondary reactions. In our case, these preliminary results indicate that NU-1000-NH_2/PrS–Cu@rGO is catalytically active

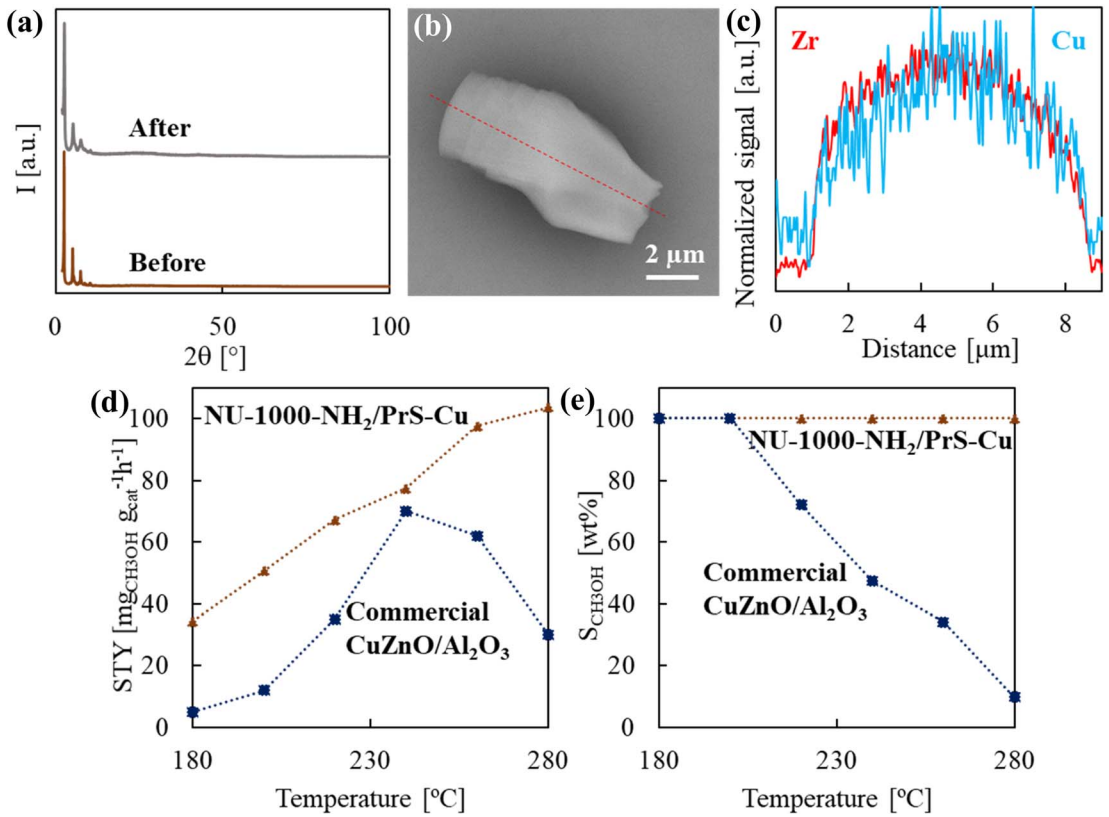

Fig. 7 Characterization and results of the sample tested for thermocatalysis: (a) PXRD of NU-1000-NH_2/PrS–Cu before and after testing, (b and c) SEM image and Zr *vs.* Cu EDS line scan of NU-1000-NH_2/PrS–Cu after testing, and (d) MeOH space-time yield (STY) and (e) MeOH selectivity (S_{CH_3OH}) of NU-1000-NH_2/PrS–Cu compared to commercial CuZnO/Al_2O_3 at the different studied temperatures.

for the electrochemical reduction of CO_2. Besides, the chronoamperometric measurements at three different potentials (−1.2 V, −1.4 V and −1.8 V *vs.* RHE, Fig. S25†) show that the measured current density is constant over time, thus suggesting that the catalyst is stable even at high negative potentials.

3.3. Thermocatalytic hydrogenation of CO_2

In the reaction of CO_2 hydrogenation, MeOH (+H_2O) can be straightforwardly obtained through the exothermic reaction of CO_2 and $3\cdot H_2$. In contrast, CO (+H_2O) is obtained in the endothermic reverse water–gas shift reaction of CO_2 and $1\cdot H_2$. Then, produced CO can exothermically react with $2\cdot H_2$ to produce more MeOH.[53] In general, the use of high temperature increases CO_2 conversion values, but it decreases the selectivity of MeOH *vs.* CO.[54] Consequently, a compromise between both factors must be attained, as the most of the laboratory and industrial processes are carried out in the temperature interval of 230–280 °C. Regarding pressure, CO_2 hydrogenation is favoured at high values, *e.g.*, 5–10 MPa, since MeOH formation entails a reduction in the number of moles. However, the use of low H_2 pressure would allow for the design of CO_2 hydrogenation processes not only economically attractive, but also energetically sustainable.[55] For these reasons, in the present work the thermocatalytic activity of NU-1000-NH_2/PrS–Cu was studied at low pressure, *i.e.*, 1 MPa, in the temperature interval of 180–280 °C.[24,56,57] The spent catalyst was characterized with regard to the structure by PXRD (Fig. 7a), the morphology by SEM and the elemental distribution of copper by EDS (Fig. 7b and c). These techniques together did not show significant modification with respect to reduced NU-1000-NH_2/PrS–Cu, thus denoting that the MOF framework, crystal morphology and copper dispersion were largely preserved during H_2 reduction and catalysis. In principle, these results point to the possibility of catalyst recycling.[58]

The catalytic activity (MeOH yield and selectivity) of the synthesized NU-1000-NH_2/PrS–Cu was compared to the frequently used industrial catalyst, developed in the 1960s for the synthesis of MeOH from CO or CO_2 and H_2 by Imperial Chemical Industries and composed of copper, zinc oxide and alumina (CuZnO/Al_2O_3).[59] In particular, CuZnO/Al_2O_3 pellets, commercialized by Alfa Group Germany (ThermoFisher) for low pressure methanol synthesis, were used.[60] Under working conditions, both studied materials produced noteworthy amounts of MeOH, although the values attained with the functionalized MOF were always superior to those with the industrial pellets (Fig. 7d). In contrast, these catalysts have a completely different behaviour with temperature. For CuZnO/Al_2O_3, the catalytic activity increases from 180 to 240 °C, but decreases at temperatures of 260 °C and higher due to sintering of the constituent NPs, which reduces copper dispersion and active surface.[61] Actually, the pelletized CuZnO/Al_2O_3 NPs are

only truly effective in a narrow temperature window settle at around 240–260 °C, with STY_{MeOH} values of 70–60 mg_{MeOH} g_{cat}^{-1} h^{-1}. In this temperature interval the selectivity of MeOH *vs.* CO was in the order of 30–50 wt%, decreasing to only 10 wt% at 280 °C with a STY_{MeOH} of 30 mg_{MeOH} g_{cat}^{-1} h^{-1} (Fig. 7e). Instead, the synthetized MOF displayed a significant activity already at a temperature as low as 180 °C (STY_{MeOH} of 35 mg_{MeOH} g_{cat}^{-1} h^{-1}), which is steadily enhanced with temperature, at least up to 280 °C (STY_{MeOH} of 103 mg_{MeOH} g_{cat}^{-1} h^{-1}). Moreover, the modified MOF displayed near 100% MeOH selectivity up to a temperature as high as 280 °C. The found noteworthy catalytic effectiveness of NU-1000-NH_2/PrS–Cu for CO_2 conversion to MeOH is related with both the favoured adsorption of CO_2 on the *ad hoc* created –NH_2 sites and the high concentration of active copper sites dispersed as individual atoms along the MOF channels. These remarkable results are also related to the huge surface area measured for NU-1000-NH_2/PrS–Cu (>1000 m^2 g^{-1}) with respect to CuZnO/Al_2O_3 (*ca.* 40 m^2 g^{-1}), which would positively affect the surface dispersion of catalytically active surface atoms of Cu^+/Cu^0, which is attained in the MOF by using a relatively low amount of copper (*ca.* 10 w%).

4 Conclusions

To obtain the desired multifunctional material for the catalytic conversion of CO_2, the framework of NU-1000 was modified with amino (–NH_2) and thiol (–PrSH) groups, installed in the linker and metal nodes, respectively. Copper active sites were added to the pores through impregnation of a Cu^{2+} salt and further reduction to obtain the NU-1000-NH_2/PrS–Cu active catalyst. This product is anticipated as a single-atom catalyst incorporating Cu^+/Cu^0 active metal sites electronically stabilized in the channels by bonding with added thiolate ($-S^-$) functionality, which avoid migration of copper atoms along the channels and their further aggregation into NPs. Additionally, high effectiveness for CO_2 conversion is expected by the favoured adsorption of the gas molecule on the *ad hoc* created –NH_2 sites, bringing CO_2 in close proximity to the catalytically active Cu^+/Cu^0 sites. Remarkably, MOF channels remain adequately accessible for the diffusion of reagents and products in a further catalytic reaction. For the target application, NU-1000-NH_2/PrS–Cu is used either as a powder in thermocatalysis or deposited on a conducting substrate in electrocatalysis. The electrocatalytic reduction of CO_2 suggested the formation of formic acid as main product. The NU-1000-NH_2/PrS–Cu is a clear example of a catalyst useful in the CO_2 hydrogenation reaction performed under mild reaction pressures, anticipated in future CO_2-to-methanol processes for safety and economic basis. A vital advantage is the extraordinary MeOH production rate at only 1 MPa (STY_{MeOH} of *ca.* 100 mg_{MeOH} g_{cat}^{-1} h^{-1} at 280 °C), which overcomes that of commercial CuZnO NPs designed for this purpose. Even more importantly, the MeOH selectivity with respect to CO can be maintained close to 100% up to temperature values of at least 280 °C, which would allow to reduce the kinetically-limited activation of the inert CO_2 molecule.

Data availability

The authors confirm that the data supporting the findings of this study are available within the article and its ESI.† Raw data were generated at UCD School of Chemistry, Materials Science Institute of Barcelona (ICMAB-CSIC), and Department of Chemical, Biological and Environmental Engineering, UAB. Derived data supporting the findings of this study are available from the corresponding author Leila Negahdar on reasonable request.

Author contributions

Albert Rosado: investigation, methodology, conceptualization, data curation, writing-original draft, funding acquisition. Ioana-Maria Popa: methodology, data curation, writing-review & editing. Eva Maria Naughton: methodology. Ahmad Abo Markeb: methodology, data curation. Javier Moral-Vico: methodology, funding acquisition. Hans-Georg Eckhardt: methodology, data curation. José A. Ayllón: conceptualization, supervision, writing – review & editing, funding acquisition. Ana M. López-Periago: conceptualization, supervision, writing – review & editing, funding acquisition. Concepción Domingo: conceptualization, supervision, writing-original draft, funding acquisition, validation. Leila Negahdar: conceptualization, supervision, writing-original draft, funding acquisition, validation.

Conflicts of interest

The authors declare no competing financial interest.

Acknowledgements

The UCD school of chemistry is acknowledged for financial support. The authors acknowledge the support of Spanish Ministry of Science and Innovation through the Severo Ochoa Program for Centers of Excellence (CEX2019-000917-S), the Spanish National Plan of Research with project PID2020-115631GB-I00 and Ecological Transition and Digital Transition Projects TED2021-1298378-C41 and TED2021-130407B-I00. A. A. Markeb is the recipient of a postdoctoral fellowship from the Spanish Ministerio de Universidades, María Zambrano ID 715364. This work has been performed in the framework of the doctoral program "Chemistry" of the UAB by A.R. that acknowledges the financial support of a FPI 2019 grant.

References

1 K. Abbass, M. Z. Qasim, H. Song, M. Murshed, H. Mahmood and I. Younis, A review of the global climate change impacts, adaptation, and sustainable mitigation measures, *Environ. Sci. Pollut. Res.*, 2022, **29**, 42539–42559.
2 A. Mardani, D. Streimikiene, F. Cavallaro, N. Loganathan and M. Khoshnoudi, Carbon dioxide (CO_2) emissions and economic growth: a systematic review of two decades of

research from 1995 to 2017, *Sci. Total Environ.*, 2019, **649**, 31–49.
3 A. V. Agbedahin, Sustainable development, education for sustainable development, and the 2030 Agenda for sustainable development: Emergence, efficacy, eminence, and future, *Sustain. Dev.*, 2019, **27**, 669–680.
4 Z. Zhang, S.-Y. Pan, H. Li, J. Cai, A. G. Olabi, E. J. Anthonyg and V. Manovic, Recent advances in carbon dioxide utilization, *Renewable Sustainable Energy Rev.*, 2020, **125**, 109799.
5 Y. Zheng, W. Zhang, Y. Li, J. Chen, B. Yu, J. Wang, L. Zhang and J. Zhang, Energy related CO_2 conversion and utilization: advanced materials/nanomaterials, reaction mechanisms and technologies, *Nano Energy*, 2017, **40**, 512–539.
6 W. Li, H. Wang, X. Jiang, J. Zhu, Z. Liu, X. Guo and C. Son, A short review of recent advances in CO_2 hydrogenation to hydrocarbons over heterogeneous catalysts, *RSC Adv.*, 2018, **8**, 7651–7669.
7 E. Nishikawa and J. Bergerson, Guiding research in electrochemical CO_2 conversion strategies through a systems-level perspective, *Green Chem.*, 2023, **25**, 229–244.
8 S. Zhang, Q. Fan, R. Xia and T. J. Meyer, CO_2 reduction: from homogeneous to heterogeneous electrocatalysis, *Acc. Chem. Res.*, 2020, **53**, 255–264.
9 J. Gao, S. C. S. Shiong and Y. Liu, Reduction of CO_2 to chemicals and fuels: thermocatalysis versus electrocatalysis, *Chem. Eng. J.*, 2023, **472**, 145033.
10 G. Pacchioni, From CO_2 to methanol on $Cu/ZnO/Al_2O_3$ industrial catalyst. What do we know about the active phase and the reaction mechanism?, *ACS Catal.*, 2024, **14**, 2730–2745.
11 S. Nitopi, E. Bertheussen, S. B. Scott, X. Liu, A. K. Engstfeld, S. Horch, B. Seger, I. E. L. Stephens, K. Chan, C. Hahn, J. K. Nørskov, T. F. Jaramillo and I. Chorkendorff, Progress and perspectives of electrochemical CO_2 reduction on copper in aqueous electrolyte, *Chem. Rev.*, 2019, **119**, 7610–7672.
12 Z. Li, S. Ji, Y. Liu, X. Cao, S. Tian, Y. Chen, Z. Niu and Y. Li, Well-defined materials for heterogeneous catalysis: from nanoparticles to isolated single-atom sites, *Chem. Rev.*, 2020, **120**, 623–682.
13 D. Yang and B. C. Gates, Catalysis by metal organic frameworks: perspective and suggestions for future research, *ACS Catal.*, 2019, **9**, 1779–1798.
14 A. Kirchon, L. Feng, H. F. Drake, E. A. Josepha and H.-C. Zhou, From fundamentals to applications: a toolbox for robust and multifunctional MOF materials, *Chem. Soc. Rev.*, 2018, **47**, 8611–8638.
15 A. Corma, H. García and F. X. Llabrés i Xamena, Engineering metal organic frameworks for heterogeneous catalysis, *Chem. Rev.*, 2010, **110**, 4606–4655.
16 H. Kima and C. S. Hong, MOF-74-type frameworks: tunable pore environment and functionality through metal and ligand modification, *CrystEngComm*, 2021, **23**, 1377–1387.
17 H. Huang, K. Shen, F. Chen and Y. Li, Metal–organic frameworks as a good platform for the fabrication of single-atom catalysts, *ACS Catal.*, 2020, **10**, 6579–6586.
18 T. Rasheed, Water stable MOFs as emerging class of porous materials for potential environmental applications, *Chemosphere*, 2023, **313**, 137607.
19 R. Abazari, S. Sanati, M. A. Bajaber, M. S. Javed, P. C. Junk, A. K. N. Jundan, J. Qian and D. P. Duba, Design and advanced manufacturing of NU-1000 metal–organic frameworks with future perspectives for environmental and renewable energy applications, *Small*, 2024, **20**, 2306353.
20 T. Islamoglu, M. A. Ortuño, E. Proussaloglou, A. J. Howarth, N. A. Vermeulen, A. Atilgan, A. M. Asiri, C. J. Cramer and O. K. Farha, Presence versus proximity: the role of pendant amines in the catalytic hydrolysis of a nerve agent simulant, *Angew. Chem., Int. Ed.*, 2018, **57**, 1949–1953.
21 P. Deria, W. Bury, J. T. Hupp and O. K. Farha, Versatile functionalization of the NU-1000 platform by solvent-assisted ligand incorporation, *Chem. Commun.*, 2014, **50**, 1965–1968.
22 C.-W. Kung, J. E. Mondloch, T. C. Wang, W. Bury, W. Hoffeditz, B. M. Klahr, R. C. Klet, M. J. Pellin, O. K. Farha and J. T. Hupp, Metal–organic framework thin films as platforms for atomic layer deposition of cobalt ions to enable electrocatalytic water oxidation, *ACS Appl. Mater. Interfaces*, 2015, **7**, 28223–28230.
23 C.-W. Kung, C. O. Audu, A. W. Peters, H. Noh, O. K. Farha and J. T. Hupp, Copper nanoparticles installed in metal–organic framework thin films are electrocatalytically competent for CO_2 reduction, *ACS Energy Lett.*, 2017, **2**, 2394–2401.
24 M. Kubovics, A. Trigo, A. Sánchez, G. Marbán, A. Borrás, J. Moral-Vico, A. M. López-Periago and C. Domingo, Role of graphene oxide aerogel support on the CuZnO catalytic activity: enhancing methanol selectivity in the hydrogenation reaction of CO_2, *ChemCatChem*, 2022, **14**, e202200607.
25 P. Li, R. C. Klet, S.-Y. Moon, T. C. Wang, P. Deria, A. W. Peters, B. M. Klahr, H.-J. Park, S. S. Al-Juaid, J. T. Hupp and O. K. Farha, Synthesis of nanocrystals of Zr-based metal–organic frameworks with csq-net: significant enhancement in the degradation of a nerve agent simulant, *Chem. Commun.*, 2015, **51**, 10925–10928.
26 J. Mao, M. Ge, J. Huang, Y. Lai, C. Lin, K. Zhang, K. Meng and Y. Tang, Constructing multifunctional MOF@rGO hydro-/aerogels by the self-assembly process for customized water remediation, *J. Mater. Chem. A*, 2017, **5**, 11873–11881.
27 D. Li, H. Liu and L. Feng, A Review on Advanced FeNi-Based Catalysts for Water Splitting Reaction, *Energy Fuels*, 2020, **34**, 13491–13522.
28 A. Rosado, O. Vallcorba, B. Vázquez-Lasa, L. García-Fernández, R. A. Ramírez-Jiménez, M. R. Aguilar, A. M. López-Periago, C. Domingo and J. A. Ayllón, Facile, fast and green synthesis of a highly porous calcium-syringate BioMOF with Intriguing triple bioactivity, *Inorg. Chem. Front.*, 2023, **10**, 2165–2173.
29 K. Kaneko, A. V. Neimark, J. P. Olivier, F. Rodriguez-Reinoso, J. Rouquerol and K. S. W. Sing, Physisorption of gases, with special reference to the evaluation of surface area and pore

size distribution (IUPAC Technical Report), *Pure Appl. Chem.*, 2015, **87**, 1051–1069.

30 I. Romero-Muñiz, C. Romero-Muñiz, I. del Castillo-Velilla, C. Marini, S. Calero, F. Zamora and A. E. Platero-Prats, Revisiting vibrational spectroscopy to tackle the chemistry of Zr_6O_8 metal-organic framework nodes, *ACS Appl. Mater. Interfaces*, 2022, **14**, 27040–27047.

31 P. Deria, J. E. Mondloch, E. Tylianakis, P. Ghosh, W. Bury, R. Q. Snurr, J. T. Hupp and O. K. Farha, Perfluoroalkane functionalization of NU-1000 via solvent-assisted ligand incorporation: synthesis and CO_2 adsorption studies, *J. Am. Chem. Soc.*, 2013, **135**, 16801–16804.

32 J. H. Kang, T.-U. Yoon, S.-Y. Kim, M.-B. Kim, H.-J. Kim, H.-C. Yang and Y.-S. Bae, Extraordinarily selective adsorption of CO_2 over N_2 in a polyethyleneimineimpregnated NU-1000 material, *Microporous Mesoporous Mater.*, 2019, **281**, 84–91.

33 L. Luconi, G. Mercuri, T. Islamoglu, G. Bergamini, Gi. Giambastiani, A. Fermi and A. Rossin, Benzothiazolium-functionalized NU-1000: a versatile material for carbon dioxide adsorption and cyanide luminescence sensing, *J. Mater. Chem. C*, 2020, **8**, 7492–7500.

34 G. Mercuri, M. Moroni, S. Galli, G. Tuci, G. Giambastiani, T. Yan, D. Liu and A. Rossin, Temperature-dependent nitrous oxide/carbon dioxide preferential adsorption in a thiazolium-functionalized NU-1000 metal–organic framework, *ACS Appl. Mater. Interfaces*, 2021, **13**, 58982–58993.

35 J. Ethiraj, E. Albanese, B. Civalleri, J. G. Vitillo, F. Bonino, S. Chavan, G. C. Shearer, K. P. Lillerud and S. Bordiga, Carbon dioxide adsorption in amine-functionalized mixed-ligand metal–organic frameworks of UiO-66 topology, *ChemSusChem*, 2014, **7**, 3382–3388.

36 K.-M. Huang, H. Tsukamoto, Y. Yong, H.-L. Chiu, M. T. Nguyen, T. Yonezawa and Y.-C. Liao, Stabilization of the thermal decomposition process of self-reducible copper ion ink for direct printed conductive patterns, *RSC Adv.*, 2017, **7**, 25095–25100.

37 F.-L. Meng, H.-X. Zhong, Q. Zhang, K.-H. Liu, J.-M. Yan and Q. Jiang, Integrated Cu_3N porous nanowire array electrode for high-performance supercapacitors, *J. Mater. Chem. A*, 2017, **5**, 18972–18976.

38 J. Jia, A. Kara, L. Pasquali, A. Bendounan, F. Sirotti and V. A. Esaulov, On sulfur core level binding energies in thiol self-assembly and alternative adsorption sites: an experimental and theoretical study, *J. Chem. Phys.*, 2015, **143**, 104702.

39 M. C. Biesinger, Advanced analysis of copper X-ray photoelectron spectra, *Surf. Interface Anal.*, 2017, **49**, 1325–1334.

40 X. Yuan, S. Chen, D. Cheng, L. Li, W. Zhu, D. Zhong, Z. Zhao, J. Li, T. Wang and J. Gong, Controllable Cu^0-Cu^+ Sites for Electrocatalytic Reduction of Carbon Dioxide, *Angew. Chem., Int. Ed.*, 2021, **60**, 15344–15347.

41 E. Cano, C. L. Torres and J. M. Bastidas, An XPS study of copper corrosion originated by formic acid vapour at 40% and 80% relative humidity, *Mater. Corros.*, 2001, **52**, 667–676.

42 C. Vericat, M. E. Vela, G. Corthey, E. Pensa, E. Cortes, M. H. Fonticelli, F. Ibanez, G. E. Benitez, P. Carro and R. C. Salvarezza, Self-assembled monolayers of thiolates on metals: a review article on sulfur-metal chemistry and surface structures, *RSC Adv.*, 2014, **4**, 27730–27754.

43 L. S. Xie, G. Skorupskii and M. Dincă, Electrically conductive metal–organic frameworks, *Chem. Rev.*, 2020, **120**, 8536–8580.

44 S. Goswami, I. Hod, J. D. Duan, C.-W. Kung, M. Rimoldi, C. D. Malliakas, R. H. Palmer, O. K. Farha and J. T. Hupp, Anisotropic redox conductivity within a metal–organic framework, *J. Am. Chem. Soc.*, 2019, **141**, 17696–17702.

45 C.-W. Kung, K. Otake, C. T. Buru, S. Goswami, Y. Cui, J. T. Hupp, A. M. Spokoyny and O. K. Farha, Increased electrical conductivity in a mesoporous metal–organic framework featuring metallacarboranes guests, *J. Am. Chem. Soc.*, 2018, **140**, 3871–3876.

46 S. Geiger, O. Kasian, A. M. Mingers, K. J. J. Mayrhofer and S. Cherevko, Stability limits of tin-based electrocatalyst supports, *Sci. Rep.*, 2017, **7**, 4595.

47 A. Korjenic and K. S. Raja, Electrochemical stability of fluorine doped tin oxide (FTO) coating at different pH conditions, *J. Electrochem. Soc.*, 2019, **166**, 169–184.

48 Z. Wang, J. Huang, J. Mao, Q. Guo, Z. Chen and Y. Lai, Metal–organic frameworks and their derivatives with graphene composites: preparation and applications in electrocatalysis and photocatalysis, *J. Mater. Chem. A*, 2020, **8**, 2934–2961.

49 M. Zhang, C. Choi, R. Huo, G. H. Gu, S. Hong, C. Yan, S. Xu, A. W. Robertson, J. Qiu, Y. Jung and Z. Sun, Reduced graphene oxides with engineered defects enable efficient electrochemical reduction of dinitrogen to ammonia in wide pH range, *Nano Energy*, 2020, **68**, 104323.

50 M. Kempasiddaiah, R. Samanta, S. Panigrahy, R. K. Trivedi, B. Chakraborty and S. Barman, Electrochemical reconstruction of a 1D Cu(PyDC)(H_2O) MOF into in situ formed Cu–Cu_2O heterostructures on carbon cloth as an efficient electrocatalyst for CO_2 conversion, *Nanoscale*, 2024, **16**, 10458–10473.

51 G. Marcandalli, M. C. O. Monteiro, A. Goyal and M. T. M. Koper, Electrolyte Effects on CO_2 Electrochemical Reduction to CO, *Acc. Chem. Res.*, 2022, **55**, 1900–1911.

52 D. Ewis, M. Arsalan, M. Khaled, D. Pant, M. M. Ba-Abbad, A. Amhamed and M. H. El-Naas, Electrochemical reduction of CO_2 into formate/formic acid: a review of cell design and operation, *Sep. Purif. Technol.*, 2023, **316**, 123811.

53 R.-P. Ye, J. Ding, W. Gong, M. D. Argyle, Q. Zhong, Y. Wang, C. K. Russel, Z. Xu, A. G. Russel, Q. Li, M. Fan and Y.-G. Yao, CO_2 hydrogenation to high-value products via heterogeneous catalysis, *Nat. Commun.*, 2019, **10**, 5698.

54 K. Cheng, Y. Li, J. Kang, Q. Zhang and Y. Wang, Selectivity control by relay catalysis in CO and CO_2 hydrogenation to multicarbon compounds, *Acc. Chem. Res.*, 2024, **57**, 714–725.

55 A. Karelovic and P. Ruiz, The role of copper particle size in low pressure methanol synthesis via CO_2 hydrogenation over Cu/ZnO catalysts, *Catal. Sci. Technol.*, 2015, **5**, 869–881.
56 A. Carrasco-García, J. Moral-Vico, A. A. Markeb and A. Sánchez, Conversion of carbon dioxide into methanol using Cu–Zn nanostructured materials as catalysts, *Nanomaterials*, 2022, **12**, 999.
57 S. Alireza-Valia, A. A. Markeba, J. Moral-Vico, X. Font and A. Sánchez, A novel Cu-based catalyst supported in chitosan nanoparticles for the hydrogenation of carbon dioxide to methanol: from the optimization of the catalyst performance to the reaction mechanism, *Catal. Commun.*, 2023, **182**, 106747.
58 M. Miceli, P. Frontera, A. Macario and A. Malara, Recovery/reuse of heterogeneous supported spent catalysts, *Catalysts*, 2021, **11**, 591–596.
59 K. C. Waugh, Methanol Synthesis, *Catal. Today*, 1992, **15**, 51–75.
60 M. Behrens, F. Studt, I. Kasatkin, S. Kühl, M. Hävecker, F. Abild-Pedersen, S. Zander, F. Girgsdies, P. Kurr and R. Schlögl, The active site of methanol synthesis over Cu/ZnO/Al_2O_3 industrial catalysts, *Science*, 2012, **336**, 893–897.
61 V. D. B. C. Dasireddy and B. Likozar, The role of copper oxidation state in Cu/ZnO/Al_2O_3 catalysts in CO_2 hydrogenation and methanol productivity, *Renewable Energy*, 2019, **140**, 452–460.